

Theory of the thermoelectric power factor in nanowire-composite matrix structures

D. A. Broido

Department of Physics, Boston College, Chestnut Hill, Massachusetts 02467, USA

N. Mingo

NASA-Ames Center for Nanotechnology, 229-1 Moffett Field, California 94035, USA

(Received 31 May 2006; revised manuscript received 23 September 2006; published 15 November 2006)

We present a theory of thermoelectric transport in nanowire-composite matrix (ncm) systems, which incorporates a complete solution of the multi-subband Boltzmann equation for inelastic carrier-phonon scattering with full calculations of the ncm electronic band structure. This theory is used to investigate the thermoelectric power factor, P_{ncm} , of ncm systems composed of InSb and PbTe. We find that P_{ncm} can be enhanced significantly compared to the bulk material, but that this enhancement depends sensitively on the carrier effective mass, on the height of the confining potential barrier that separates the ncm from the nanowires, and on the cross-sectional size of the ncm relative to that of the nanowires. These results suggest that care must be taken in the choice of ncm material as well as that of the nanowires in order to optimize the thermoelectric power factor of nanowire-composite structures.

DOI: [10.1103/PhysRevB.74.195325](https://doi.org/10.1103/PhysRevB.74.195325)

PACS number(s): 73.50.Lw, 73.63.-b, 73.50.Dn

I. INTRODUCTION

Intense research has been ongoing in recent years to identify nanostructured materials for thermoelectric applications.¹⁻¹⁸ Among the systems being investigated are confined systems such as nanowire superlattices,^{6,7,15,16} in which periodically arranged wire conducting regions are separated by a matrix material. The matrix provides required stability for the nanowire array, and it produces confinement effects that can enhance the thermoelectric properties of the nanowires. In some previous theoretical work,^{2,8,14,17} only the thermoelectric properties of individual nanowires were studied, and the supporting matrix structure was not considered. In other work,^{10,11,15,16} the matrix was taken to be an insulator with poor thermoelectric properties. Compared to the free-standing wires, this matrix, therefore, had a parasitic effect on the thermoelectric efficiency of the full nanowire-composite structure, which could in fact be lower than that of the corresponding bulk thermoelectric material. An alternative approach would be to use a matrix that is itself composed of an optimized thermoelectric material. By optimizing the thermoelectric properties of both the nanowire and the surrounding matrix in a nanowire-composite structure, the thermoelectric properties of this structure could be significantly improved compared to either bulk constituent.

The thermoelectric power factor, P , is a key determinant of the efficiency of a material for thermoelectric applications. It is the product of the electrical conductivity, σ , and the square of the Seebeck coefficient, S : $P = \sigma S^2$. With increasing carrier density, σ increases while S decreases so that for a given material system P exhibits a peak at the optimum carrier density. This optimized P has been studied theoretically in a variety of nanoscale structures.^{13-16,18} Recent work¹⁸ focused on calculations of the power factor for a nanowire-composite matrix perforated by a periodic array of nanowire pores. That work clarified the qualitative dependence of the power factor for such matrix structures and estimated the enhancements due to confinement effects. In that study, the interfaces between the matrix material and the empty space

in the nanowire pores was represented by infinite potential barriers. In addition, the scattering of carriers was taken to be represented by a constant relaxation time. While that work demonstrated significant increases in the power factor, it raises the question of the robustness of this enhancement when a more realistic microscopic treatment is used.

In the present work, we develop and examine the results of such a treatment. Specifically, we take the potential barrier experienced by carriers in the matrix material to be finite rather than infinite. This allows the carrier wave functions to penetrate into the nanowire pores. In addition, instead of using the constant relaxation time approximation (CRTA) for the carrier scattering, we employ an accurate treatment of the dominant scattering mechanisms for electrons at room temperature. We develop a theory of thermoelectric transport in nanowire-composite matrix structures that includes inelastic carrier scattering by polar optic phonons through the Fröhlich interaction and the elastic scattering of carriers by acoustic phonons through the deformation potential interaction. We calculate the power factor of nanowire-composite matrix structures composed of two thermoelectric materials, InSb and PbTe, which we find to represent a range of behaviors, described in detail below. We examine the size and temperature dependence of the power factor in these matrix systems. We demonstrate important features of the power factor of nanocomposite matrix structures that emerge from the rigorous treatment presented here. We show that through judicious choice of materials and structures the power factor of the nanowire nanocomposite matrix itself can be enhanced compared to the bulk thereby adding to potential power factor increases in the nanowires themselves.

II. THEORY

We focus on the thermoelectric properties of the matrix portion of a nanowire-composite structure. We consider a nanocomposite matrix material penetrated periodically by nanowire pores with square cross-section. A cross-section of

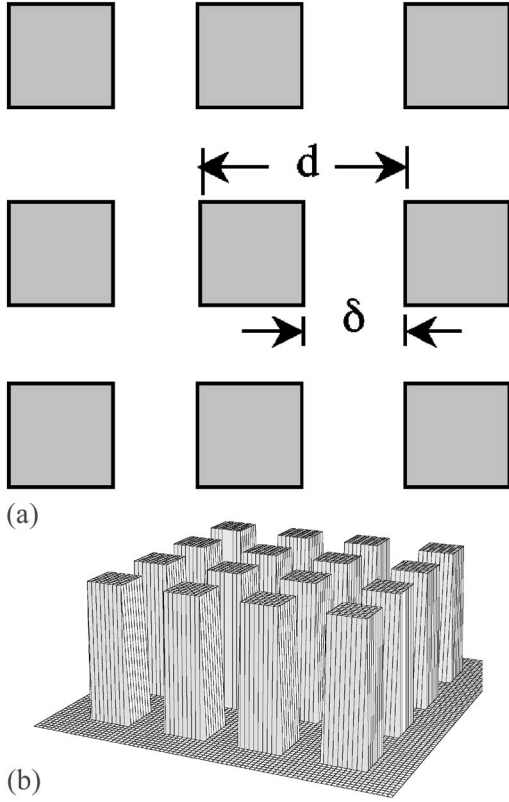


FIG. 1. (a) Cross section of a nanowire-composite matrix structure. The shaded square regions represent nanowire pores, while the white regions show the matrix cross section. In each direction, d is the period and δ is the separation between nanowire pores. (b) Potential energy profile for a carrier in the matrix. Nanowire pores produce periodic potential barriers of square cross section and of height, V_0 .

such a structure is shown in Fig. 1(a). The period in each direction is d , while the separation between nanowire pores is δ . In the matrix region, we take the potential energy seen by a conduction electron to be zero,¹⁹ while the nanowire pores are taken to produce a potential barrier of height, V_0 . The potential profile is then that of a two-dimensional Kronig-Penney model, illustrated schematically in Fig. 1(b). A conduction electron moving through the matrix will experience confinement effects. The state of such an electron is specified by a subband index, n , and by a wave vector, \mathbf{k} .

We consider thermoelectric transport in the matrix along the axis of the nanowire holes and perpendicular to the cross section in Fig. 1(a). A small electric field, $\mathbf{E} = E_z \hat{z}$, and temperature gradient, $\nabla T = (dT/dz) \hat{z}$, are taken to be applied along this direction, which we define as the z -direction. The Boltzmann equation that describes this transport is

$$-\frac{e\mathbf{E}}{\hbar} \cdot \nabla_{\mathbf{k}} f_n + \frac{\nabla_{\mathbf{k}} \varepsilon_n}{\hbar} \cdot \nabla T \frac{\partial f_n}{\partial T} = \left. \frac{\partial f_n}{\partial t} \right|_{\text{coll}}, \quad (1)$$

$$\left. \frac{\partial f_n}{\partial t} \right|_{\text{coll}} = \frac{V}{8\pi^3} \sum_{n'} \int d\mathbf{k}' [W_{n'n}(\mathbf{k}', \mathbf{k}) f_{n'}(\mathbf{k}') (1 - f_n(\mathbf{k})) - W_{nn'}(\mathbf{k}, \mathbf{k}') f_n(\mathbf{k}) (1 - f_{n'}(\mathbf{k}'))]. \quad (2)$$

Here, $f_n(\mathbf{k}, \mathbf{r})$ is the distribution function for electrons in

nanocomposite matrix state (n, \mathbf{k}) , $W_{nn'}(\mathbf{k}, \mathbf{k}')$ is the scattering rate taking electrons from state (n, \mathbf{k}) to state (n', \mathbf{k}') , and $\varepsilon_n(\mathbf{k})$ is the electron energy. The collision operator, $\partial f_n / \partial t|_{\text{coll}}$, accounts for intra- and inter-subband elastic and inelastic scattering into and out of the state (n, \mathbf{k}) .

The distribution function for the n th nanocomposite matrix subband can be expressed in terms of its deviation, δf_{nk} , from the equilibrium (Fermi) distribution, f_0 : $f_{nk} = f_0 + \delta f_{nk}$, with²⁰

$$\delta f_{nk} = \left(\frac{\partial f_0}{\partial \varepsilon} \right) v_z \left(e E_z \tau_{1n}(\mathbf{k}) + \frac{1}{T} \frac{dT}{dz} \tau_{2n}(\mathbf{k}) \right). \quad (3)$$

The scattering functions, $\tau_{1n}(\mathbf{k})$ and $\tau_{2n}(\mathbf{k})$, are anisotropic reflecting the anisotropic and non-parabolic matrix band structure. Substituting Eq. (3) into the Boltzmann equation leads to two sets of coupled equations for these scattering functions. These equations can be solved iteratively, as described in detail in Ref. 16 for given electron dispersions and scattering mechanisms.

We consider matrix materials with isotropic and parabolic bulk electron dispersions. The energies for electrons in the matrix structure are then

$$\varepsilon_n(\mathbf{k}) = \varepsilon_n(k_x, k_y) + \frac{\hbar^2 k_z^2}{2m^*} \quad (4)$$

where $\varepsilon_n(k_x, k_y)$ is the non-parabolic and anisotropic part of the dispersion resulting from the two-dimensional periodic nanowire pore potential shown in Fig. 1(b). We obtain $\varepsilon_n(k_x, k_y)$ along with the corresponding Bloch functions by solving the Schrödinger equation for this two-dimensional Kronig-Penney potential with offset V_0 . We write the carrier Bloch functions as $\psi_{nk}(\mathbf{r}) = e^{ik_z z} \psi_{nk\perp}(\boldsymbol{\rho})$ where $\psi_{nk\perp}(\boldsymbol{\rho}) = e^{i\mathbf{k}\perp \cdot \boldsymbol{\rho}} u_{nk\perp}(\boldsymbol{\rho})$, with $\boldsymbol{\rho} = (x, y)$. The periodic part of the Bloch function, $u_{nk\perp}(\boldsymbol{\rho})$, is expanded in a basis of products of Bloch states for the one-dimensional Kronig-Penney model: $u_{nk\perp}(\boldsymbol{\rho}) = \sum_{n_1 n_2} c_{nk\perp}(n_1, n_2) u_{n_1 k_x}(x) u_{n_2 k_y}(y)$, where $u_{n_1 k_x}(x)$ and $u_{n_2 k_y}(y)$ satisfy $u_{nk_x}(x+d) = u_{nk_x}(x)$ and $u_{nk_y}(y+d) = u_{nk_y}(y)$ and can be expressed analytically.²¹

The dominant scattering mechanisms for carriers around room temperature in many semiconductors are: (1) Carrier-Polar optic phonon scattering (pop) through the Fröhlich interaction and (2) Carrier-acoustic phonon scattering (ac) via the deformation potential interaction. We take the phonons to be unaffected by the matrix potential. In confined systems the scattering rates by optic phonons have been shown to be given to a good approximation by bulk plane waves for the phonons,^{22,23} and the matrix potential structuring has only small effects on the acoustic phonons. We take the optic phonon branch to be dispersionless and given by its zone center value, $\hbar\omega_0$, and the acoustic branch is taken to be linear with an averaged isotropic velocity, v_0 . Then the pop electron-phonon scattering rate for the nanowire-composite matrix is²⁴

$$W_{nn'}^{\text{pop}}(\mathbf{k}, \mathbf{k}') = \frac{2\pi}{\hbar} \left(n_0 + \frac{1}{2} \pm \frac{1}{2} \right) C_{\text{pop}}^2 M_{nn'}^{\text{pop}}(\mathbf{k}, \mathbf{k}') \delta(\varepsilon_n(\mathbf{k}') - \varepsilon_n(\mathbf{k}) \pm \hbar\omega_0), \quad (5)$$

$$M_{nn'}^{\text{pop}}(\mathbf{k}, \mathbf{k}') = \sum_{m_1, m_2} \frac{|F_{n\mathbf{k}_\perp n'\mathbf{k}'_\perp}(K_{m_1}, K_{m_2})|^2}{(\Delta k_x + K_{m_1})^2 + (\Delta k_y + K_{m_2})^2 + \Delta k_z^2}. \quad (6)$$

Here, $C_{\text{pop}}^2 = 2\pi e^2 \omega_0 / \kappa^* V$ measures the strength of the pop scattering, the $+$ ($-$) sign is for pop phonon emission (absorption), the $\Delta k_i = k_i' - k_i$ with $i=x, y, z$ reflect the change in the electron wave vector in the scattering process, $\mathbf{K} = (K_{m_1}, K_{m_2})$ with $K_m = 2\pi m/d$ is the reciprocal lattice vector of the ncm, $1/\kappa^* = 1/\kappa_\infty - 1/\kappa_0$, with κ_0 (κ_∞) being the static (high frequency) dielectric constant, $n_0 = 1/\exp((\hbar\omega_0/k_B T) - 1)$, and V is the crystal volume. The overlap factor is

$$F_{n\mathbf{k}_\perp n'\mathbf{k}'_\perp}(\mathbf{K}) = \int_{\text{Cell}} e^{i(\mathbf{k}'_\perp - \mathbf{k}_\perp - \mathbf{K}) \cdot \boldsymbol{\rho}} \psi_{n'\mathbf{k}'_\perp}^*(\boldsymbol{\rho}) \psi_{n\mathbf{k}_\perp}(\boldsymbol{\rho}) d\boldsymbol{\rho}. \quad (7)$$

For scattering of electrons by acoustic phonons we exploit the fact that the average electron energy around room temperature is considerably larger than that of acoustic phonons involved in the deformation potential scattering. Thus, the scattering rate for this mechanism is, to good approximation, elastic, and takes on the high temperature form¹⁶

$$W_{nn'}^{ac}(\mathbf{k}, \mathbf{k}') = \frac{2\pi}{\hbar} C_{ac}^2 M_{nn'}^{ac}(\mathbf{k}_\perp, \mathbf{k}'_\perp) \delta(\varepsilon_{n'}(\mathbf{k}') - \varepsilon_n(\mathbf{k})) \quad (8)$$

with

$$M_{nn'}^{ac}(\mathbf{k}_\perp, \mathbf{k}'_\perp) = \sum_{m_1, m_2} |F_{n\mathbf{k}_\perp n'\mathbf{k}'_\perp}(K_{m_1}, K_{m_2})|^2. \quad (9)$$

Here the deformation potential scattering strength $C_{ac}^2 = E_1^2 k_B T / 2V\rho v_0^2$ depends on the deformation potential of the material, E_1 , the density, ρ , and the averaged acoustic velocity, v_0 .

For each matrix structure considered, we calculate the scattering rates from Eqs. (5)–(9). Using these, we convert the multi-subband inelastic Boltzmann equation, Eqs. (2) and (3) into a set of coupled equations for the scattering functions, $\tau_{1n}(\mathbf{k})$ and $\tau_{2n}(\mathbf{k})$, which we solve iteratively. Details of this iterative procedure have been described previously.¹⁶ This allows us to calculate the power factor for the nanowire-composite matrix structure, which we can express as

$$P(\mu) = \frac{k_B^2}{m^* \pi^2 d^2} \left(\frac{2m^* k_B T}{\hbar^2} \right)^{1/2} \frac{I_1^2}{I_0}, \quad (10)$$

$$I_0 = \frac{1}{\pi^2} \sum_n \int_0^\pi d\alpha_x \int_0^\pi d\alpha_y \int_0^\infty dx \frac{-df_0}{dx} x^{1/2} \tau_{1n} \times \left(\frac{\alpha_x}{d}, \frac{\alpha_y}{d}, \frac{2m^* x}{\hbar^2 \beta} \right) dx, \quad (11)$$

$$I_1 = \frac{1}{\pi^2} \sum_n \int_0^\pi d\alpha_x \int_0^\pi d\alpha_y \int_0^\infty dx \frac{-df_0}{dx} x^{1/2} (x - \zeta_n) \tau_{1n} \times \left(\frac{\alpha_x}{d}, \frac{\alpha_y}{d}, \frac{2m^* x}{\hbar^2 \beta} \right) dx, \quad (12)$$

where $\alpha_x = k_x d$, $\alpha_y = k_y d$, $x = (\varepsilon - \varepsilon_n(k_x, k_y))\beta$, $f_0 = f_0(x, \zeta_n(k_x, k_y))$, and where $\zeta_n(k_x, k_y) = (\mu - \varepsilon_n(k_x, k_y))\beta$ is the scaled chemical potential. We note that only the scattering functions, τ_{1n} , are needed to calculate the power factor. The functions τ_{2n} enter in the calculation of the electrical component of the thermal conductivity, which is not considered here. We also note that the power factor, P , is a function of the chemical potential, μ , and so of the carrier density. In all cases considered below, we calculate the $\mu = \mu_{\text{max}}$ that gives the maximum power factor, $P_{ncm} = P(\mu_{\text{max}})$.

III. RESULTS AND DISCUSSION

We examine the thermoelectric power factor of nanowire-composite matrix structures composed of InSb and PbTe. These materials provide a range of effective masses and relative strengths of the two electron-phonon scattering mechanisms considered. InSb has a single isotropic conduction band valley, which we take to be parabolic.²⁵ We take the following material parameters for InSb: $m^* = 0.0155$, $E_1 = 9.5$ eV, $\hbar\omega_0 = 24.0$ meV, $\varepsilon_0 = 17.64$, $\varepsilon_\infty = 15.75$, $\rho v_0^2 = 524$ meV \AA^3 .²⁶ The conduction band of bulk PbTe has four equivalent anisotropic valleys along the [111] directions. The material parameters for PbTe are taken to be $m_\ell = 0.35$, $m_t = 0.034$, and $E_1 = 25$ eV, $\hbar\omega_0 = 14$ meV, $\varepsilon_0 = 414$, $\varepsilon_\infty = 33$, and $\rho v_0^2 = 486$.^{27,28} Here, m_ℓ and m_t are the longitudinal and transverse masses for the [111] valleys. We consider the orientation of the ncm so that the confinement directions are along [100] and [010]. The confinement masses along these two directions are both equal to 0.049 so that the valley degeneracy is retained for all ncm subbands.¹⁶ We take the same effective mass along the z direction. It has been observed that the effective mass of electrons in PbTe exhibits a strong temperature dependence,²⁹ increasing by roughly 25% per 100 K in the temperature range of interest. When considering the temperature dependence of the power factor of PbTe (see Fig. 8 and accompanying discussion), we incorporate this behavior in the following way. At 300 K, we take the mass determined above of 0.49. At 200 and 400 K we take the effective masses to be $0.049/1.25 = 0.039$ and $0.049 \times 1.25 = 0.061$.

For each material we fix a cross-sectional ratio, d/δ , and we choose a barrier height, V_0 , and a temperature, T . The power factor is then optimized as a function of carrier density for each d . For simplicity, the nanowire barrier region is taken to have the same material parameters as the matrix region. Roughly, this amounts to taking the nanowire pores to be filled with a high-barrier material. Since we are interested in the thermoelectric properties of the matrix material, we multiply our calculated power factor for the full structure whose volume, V_{bulk} , includes the high-barrier region by V_{Bulk}/V_{ncm} where V_{ncm} is the volume occupied by just the matrix. For the two cases considered below of $d/\delta = 2$ and

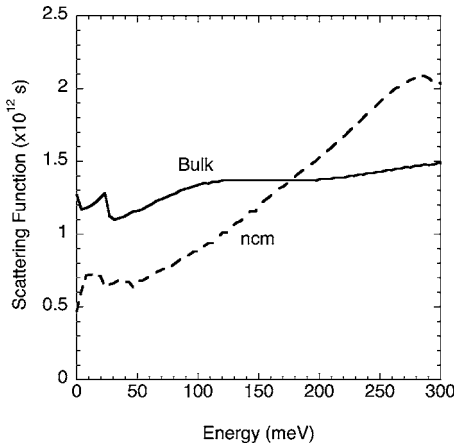


FIG. 2. Scattering function for the first subband of an InSb nanowire nanocomposite structure, $\tau_{11}(k_x=0, k_y=0, \varepsilon)$, with $T=300$ K, $V_0=3$ eV, and $d=2\delta=120$ nm compared to the scattering function for bulk InSb.

$d/\delta=4$ the volume scaling factors are $V_{\text{Bulk}}/V_{\text{ncm}}=4/3$ and $V_{\text{Bulk}}/V_{\text{ncm}}=16/7$, respectively.

To better understand the iterative approach used here, we first discuss the behavior of the scattering functions, τ_1 . Figure 2 compares the bulk InSb scattering function with the zone center scattering function for the first subband of an InSb nanowire nanocomposite structure, $\tau_{11}(k_x=0, k_y=0, \varepsilon)$, with $T=300$ K, $V_0=3$ eV, and $d=2\delta=120$ nm. This choice of parameters corresponds to relatively strong confinement, in which the lowest subband provides the dominant contribution and a large power factor is achieved, as seen below in Fig. 5. The effect of the composite structure on the scattering function is evident: $\tau_{11}(k_x=0, k_y=0, \varepsilon)$ is relatively flat for low energy, similar to the bulk case, but then increases at high energy. This reflects the fact that at lower energy, the electronic dispersion of the *ncm* is three-dimensional (3D), but at higher energy, it becomes one-dimensional, and the lack of intersubband scattering gives a higher τ_{11} at high energy than is the case for the bulk τ_1 . We note that as discussed below, bulk-like behavior is expected for both large and small d , and for small confinement, V_0 . For small d , barrier penetration causes the dispersion to be 3D for even high energies yielding a bulk-like τ_{11} ; for large d , the subbands overlap, intersubband scattering becomes significant and again the bulk-like behavior is recovered.

Figure 3 shows the electronic density of states (solid line) for the first subband of the InSb nanowire nanocomposite structure considered in Fig. 2, compared to that of bulk InSb (dotted line) and that for fully one-dimensional confinement, corresponding to $\varepsilon_n(k_x, k_y)=\varepsilon_n=\text{constant}$ (dashed line). As we have taken the bulk material to have isotropic and parabolic dispersion, the bulk density of states is proportional to $\varepsilon^{1/2}$ while the one-dimensional density of states is proportional to $\varepsilon^{-1/2}$. The *ncm* density of states exhibits a more complex structure. For low energy it matches that of the bulk material reflecting the initial parabolicity of $\varepsilon_n(k_x, k_y)$. For increasing energy, the nonparabolic flattening of $\varepsilon_n(k_x, k_y)$ causes the density of states to increase above the bulk value. For energy increasing above $\varepsilon_n(k_x, \pi/d)$ the dimensionality

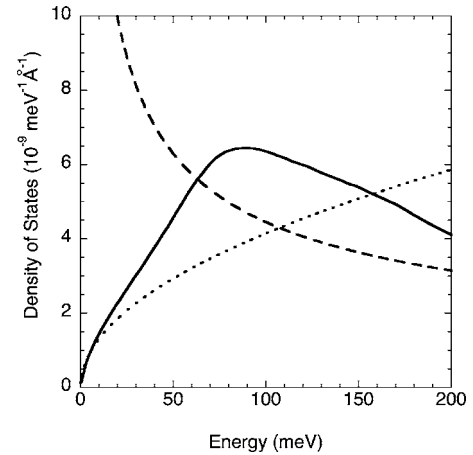


FIG. 3. Electronic density of states for an InSb nanowire nanocomposite structure with $V_0=3$ eV, and $d=2\delta=120$ nm (solid line) compared with that for bulk InSb (dotted line) and that for strictly one-dimensional confinement (dashed line).

is reduced, and the density of states approaches the one-dimensional case until the energy of the next subband is reached. The maximum power factor for this case occurs for a chemical potential around $\mu \approx 150$ meV. The enhancement in the *ncm* density of states for energies below this compared to the bulk case offsets the reduction in the *ncm* scattering function observed in Fig. 2 and leads to an increase in the electrical conductivity and the consequent increase in power factor illustrated in Fig. 5.

It is of interest to consider the dependence of the scattering functions on the strength of the two electron scattering mechanisms (ac and pop). The pop scattering strength is governed by the optic phonon energy, $\hbar\omega_0$, while the ac scattering strength depends on the deformation potential, E_1 . Figure 4 shows the zone-center scattering function from the first subband $\tau_{11}(k_x=0, k_y=0, \varepsilon)$ calculated for the InSb *ncm* with $T=300$ K, $V_0=3$ eV, and $d=2\delta=120$ nm (the same parameters used in Fig. 2), but for the two cases: (1) no ac scattering: $\hbar\omega_0$ unchanged, $E_1=0$ (solid line), and (2) no pop

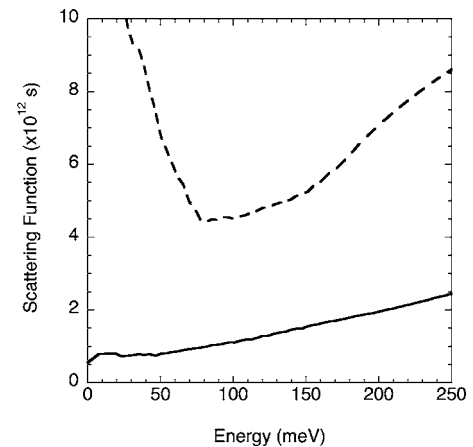


FIG. 4. Scattering functions for the first subband of an InSb nanowire nanocomposite structure, $\tau_{11}(k_x=0, k_y=0, \varepsilon)$, with $T=300$ K, $V_0=3$ eV, and $d=2\delta=120$ nm; solid line is calculated ignoring pop scattering; dashed is calculated ignoring ac scattering.

scattering: $\hbar\omega_0=0$, E_1 unchanged (dashed line). For InSb, ac scattering is weak, and the behavior of the power factor is dominated by the pop scattering. This is evidenced by the fact that the τ_{11} for case 2 is considerably larger than it is for case 1, with τ_{11} for case 1 being quite close to the combined τ_{11} in Fig. 2.

The form of τ_{11} for case 2 can be understood as follows. For the elastic ac scattering, τ_{11} scales inversely with the density of states (DOS) of the first subband, D_1 .¹⁸ At low energy electron experiences a roughly 3D DOS as seen in Fig. 3. Since the 3D DOS is proportional to $\varepsilon^{1/2}$, $\tau_{11} \sim \varepsilon^{-1/2}$, which is the low energy behavior exhibited in Fig. 4. At higher energy, above $\varepsilon_1(\pi/d, \pi/d)$, the DOS becomes one-dimensional, scaling as $\varepsilon^{-1/2}$ and giving $\tau_{11} \sim \varepsilon^{1/2}$ as seen in Fig. 4. For case 2 (ac scattering only), we find a much weaker dependence of the power factor, p_{ncm} on d , and much smaller enhancement in p_{ncm} over the bulk value compared to that seen in Fig. 5 below. This is because the electrical conductivity, σ , scales as $\sigma \sim D_1 \tau_{11}$ as does σS , so that $P_{ncm} = (\sigma S)^2 / \sigma \sim D_1 \tau_{11}$. In the limit of full confinement [$\varepsilon_n(k_x, k_y) = \varepsilon_n = \text{constant}$] the dispersion becomes purely one-dimensional so that $D_1 \sim 1/d^2$. Since $\tau_{11} \sim 1/D_1$, p_{ncm} is then independent of d in this limit.¹⁸ Such full confinement is in fact not achieved in the *ncm* thus allowing p_{ncm} for this case exhibit a weak dependence on d .

Figure 5 shows the optimized power factor P_{ncm} for an InSb nanocomposite matrix plotted as a function of d for $V_0=3$ eV, $T=300$ K and for the two cross-sectional ratios $d/\delta=2$ (solid line) and $d/\delta=4$ (dashed line). The power factors are scaled to the optimized room temperature power factor calculated for bulk InSb. For large d , P_{ncm} is near the bulk value for both cases. This is expected because for sufficiently large d , the mean free path of the carriers becomes larger than δ , and the power factor of the matrix material should converge to the bulk value. In our previous work within the CRTA,¹⁸ we have found that this limit is achieved for $d > 100$ nm. The complexity of the model considered in the present work precludes our calculating P_{ncm} for such large values of d .³⁰

For decreasing d , P_{ncm} first increases and then exhibits a peak. The increase in P_{ncm} occurs because as d is reduced the

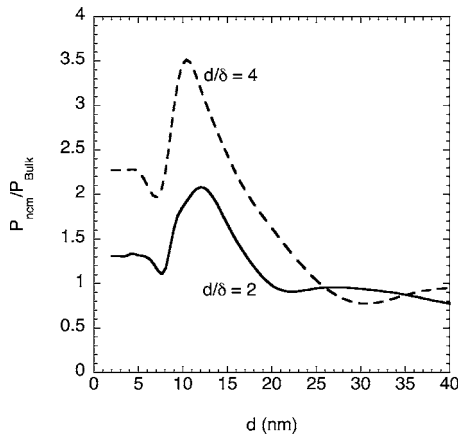


FIG. 5. Power factor of nanowire nanocomposite matrix structures composed of InSb for $T=300$ K, $V_0=3$ eV, and for two values of d/δ as a function of the period, d .

separation between electronic subbands increases, intersubband scattering becomes negligible and the system begins to take on quasi-1D behavior, with properties dominated by a single subband with small k_x-k_y dispersion. The carrier density of states then scales roughly as $1/d^2$, and this causes the electrical conductivity and so the power factor to increase with decreasing d . We note that this enhancement is the fortuitous result of the weakness of the *ac* scattering compared to the pop scattering. The *ac* scattering rate scales inversely with the density of states causing the *ac* scattering-limited electrical conductivity not to increase with decreasing d .¹⁶ However, since the *ac* scattering is significantly weaker in InSb than the pop scattering this limit corresponds to extremely large values of the power factor, which are never reached because of the decrease in P_{ncm} observed for small d in Fig. 5.

This small d behavior occurs for two reasons: First, the *ncm* Brillouin zone size scales as $1/d$, and for small d , the band width of the lowest subband, $\varepsilon_1(k_x=\pi/d, k_y=\pi/d) - \varepsilon_1(k_x=0, k_y=0)$, is so large that the carriers essentially sample a three-dimensional band structure leading to a reduction in P_{ncm} . Second, as $d \rightarrow 0$, barrier penetration of the carrier wave functions in the *ncm* into the nanowire pore regions becomes significant. This causes the power factor to decrease. For sufficiently small d , the charge density is able to spread throughout the whole structure as if the barriers were not present, so that the bulk power factor is recovered. In Fig. 5, in the $d \rightarrow 0$ limit, P_{ncm} converges to $4/3$ for $d/\delta=2$ and $16/7$ for $d/\delta=4$. If we divide these values by the corresponding volume scaling factors defined above, we see that in both cases the bulk result is indeed obtained.

We note that there is a significant enhancement in the peak value of P_{ncm} when the cross-sectional ratio, d/δ , is doubled with the peak value for $d/\delta=4$ being about 1.7 times that for $d/\delta=2$ and more than three times larger than the bulk value. To understand this we note that for given d , the cross-sectional ratio is increased by reducing δ . The onset for quasi-one dimensional behavior and corresponding power factor enhancement is determined by δ , so that, in principle, as $d/\delta \rightarrow \infty$ the peak in P_{ncm} can be made very large. We have verified this behavior in our previous work for infinite barriers.¹⁸ However, we note that for the realistic finite barrier case considered here, wave function penetration into the barrier region strongly suppresses P_{ncm} . This is evident by noting that for the infinite barrier case, $V_0=\infty$, the peak power factor obtained for $d/\delta=4$ is about 3.3 times larger than for $d/\delta=2$. This is roughly twice that obtained here for $V_0=3$ eV.

The sensitivity of the peak value of P_{ncm} to barrier height is highlighted further in Fig. 6, which shows the optimized P_{ncm} for InSb with $d/\delta=2$, $T=300$ K and for three different barrier heights, $V_0=3$ eV, $V_0=1$ eV, and $V_0=0.5$ eV. With decreasing barrier height, the peak value of P_{ncm} drops precipitously. This reflects the fact that with decreasing V_0 , the density of states and the scattering functions approach their bulk form. This suggests that large barriers between the matrix material and the nanowires is essential in order to maximize enhancement of the power factor in nanowire-composite structures.

In Fig. 7(a), the optimized P_{ncm} for InSb is plotted versus d for $d/\delta=2$, $V_0=3$ eV, and for three different temperatures.

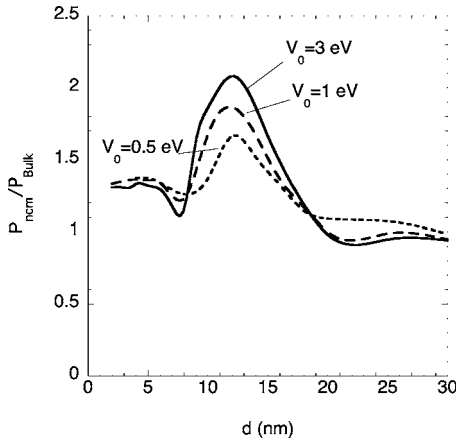
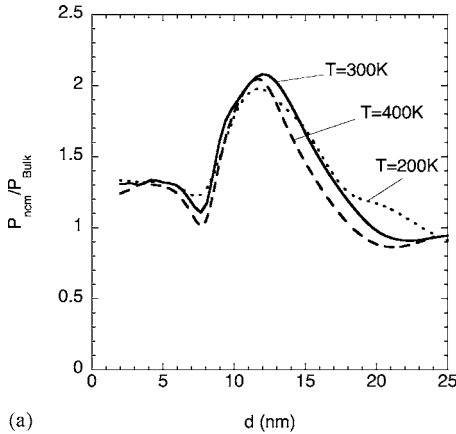
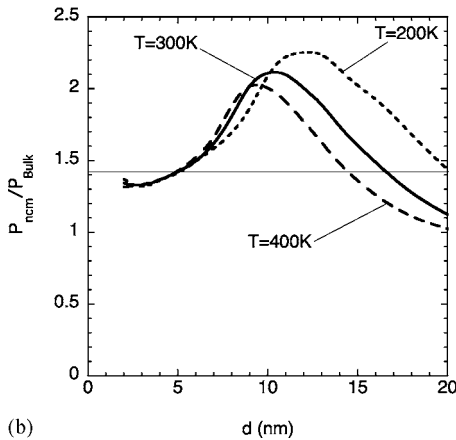


FIG. 6. Power factor of nanowire nanocomposite matrix structures composed of InSb for $d/\delta=2$, $T=300$ K, and for three values of barrier offset V_0 as a function of the period, d .

Note that the three curves are almost identical, with the peak positions exhibiting little temperature dependence. This is to be contrasted with Fig. 7(b), which shows the nanowire-composite matrix power factor calculated in the constant



(a)



(b)

FIG. 7. (a) Power factor of nanowire nanocomposite matrix structures composed of InSb for $d/\delta=2$, $V_0=3$ eV, and for three different temperatures, as a function of the period, d . (b) Power factor as in (a) but calculated within the constant relaxation time approximation.

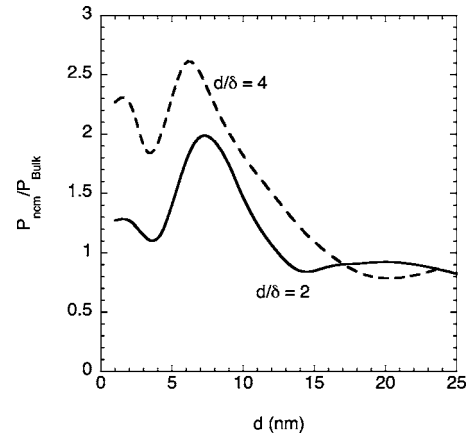


FIG. 8. Power factor of nanowire nanocomposite matrix structures composed of PbTe for $T=300$ K, $V_0=3$ eV, and for two values of d/δ as a function of the period, d .

relaxation time approximation. Here, a strong temperature dependence is evident with the peak shifting to lower d . The reason for the shift in the curves with temperature has been explained¹⁸ through a universal scaling relation of the ncm power factor depending on d , carrier effective mass, and temperature. This scaling relation is well fit for the large d portion of the curves beyond the peak positions. This relation predicts that the same value of P_{ncm} should be obtained when $d_1/d_2 = \sqrt{T_1/T_2}$.¹⁸ The intersection of the three curves in Fig. 7(b) with the thin horizontal line indeed follow this relation closely. However, around and below the peak positions, this is no longer true because wave function penetration into the barrier region decreases the power factor for small d , thus producing a premature peak of reduced height and at larger d than would be obtained from an infinite barrier theory. When the dominant scattering mechanism for carriers in InSb (inelastic pop scattering) is introduced, the universal scaling behavior is no longer obeyed for any value of d .

Figure 8 shows the optimized power factor P_{ncm} for an PbTe[100]-oriented nanocomposite matrix plotted as a function of d for $V_0=3$ eV, $T=300$ K, and for the two ratios $d/\delta=2$ (solid line) and $d/\delta=4$ (dashed line). Note that the curves exhibit peaks at smaller values of d than occurs for the case of InSb shown in Fig. 5. This shift occurs because of the larger effective mass in PbTe. With increasing carrier effective mass, the value of d , below which a single subband dominates the transport, decreases, and it is this region in which the density of states and the scattering functions acquire their quasi-one-dimensional form, and the resulting enhancement in P_{ncm} occurs. For $d/\delta=4$, the enhancement in the peak value of P_{ncm} is considerably reduced compared to that for InSb observed in Fig. 4. This can be understood as follows. For the infinite barrier case,¹⁸ the peak position in P_{ncm} shifts to lower d with increasing d/δ . Because of wave function penetration into the barriers, the peak for $d/\delta=4$ is not able to fully form, as was also the case for InSb (see Fig. 5). This effect is more exaggerated for PbTe than for InSb because the barrier penetration effects are more strongly dependent on d for small d . We note here that GaAs has a larger effective mass than either InSb or PbTe, and our calculated power factors for GaAs ncm 's (not shown here)

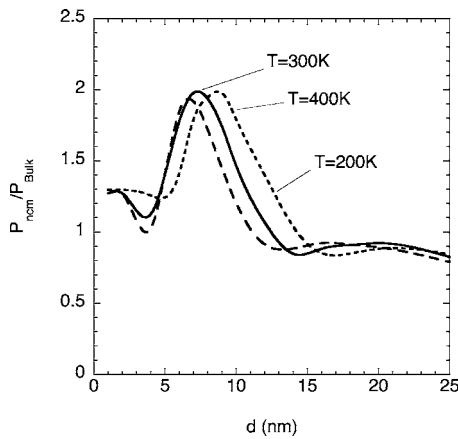


FIG. 9. Power factor of nanowire nanocomposite matrix structures composed of PbTe for $d/\delta=2$, $V_0=3$ eV, and for three different temperatures, as a function of the period, d .

exhibit peaks below 5 nm and peak values of P_{ncm} that are noticeably lower than those for InSb and PbTe, consistent with the above reasoning.

Figure 9 shows the optimized power factor P_{ncm} for an PbTe[100]-oriented nanowire-composite matrix plotted as a function of d for $V_0=3$ eV, and for three different temperatures. Note that in contrast to the case of InSb shown in Fig. 7(a), in PbTe the peak position exhibits a noticeable temperature dependence. In InSb, the inelastic pop scattering is stronger than the ac scattering and so dominates the behavior of the power factor around room temperature. In PbTe, the large dielectric constants and small zone center LO phonon energy weaken the inelastic pop scattering, while the large deformation potential strengthen the elastic ac scattering. This produces a noticeable temperature dependence closer to that predicted from the CRTA.¹⁸ In addition, the strong temperature dependence of the effective mass in PbTe²⁹ shifts the curve for 400 K slightly to smaller d and that for 200 K

to larger d , thus enhancing the temperature dependence of P_{ncm} .

IV. SUMMARY AND CONCLUSIONS

We have developed a theory of the thermoelectric power factor of nanowire-composite matrix systems. Our theory incorporates both inelastic scattering of carriers by polar optic phonons and elastic scattering of carriers through the deformation potential interaction, which are the dominant carrier scattering processes in many semiconductor materials around room temperature. We find that under appropriate conditions the power factor of the ncm can be substantially enhanced compared to the bulk material. Materials with small effective mass such as InSb give peak enhancement at larger ncm period, d , thereby minimizing detrimental barrier penetration effects. We show that for materials in which inelastic pop scattering is dominant, such as InSb, the position and magnitude of the peak are stable against changes in temperature. We find that larger potential barriers, V_0 , separating the ncm from the nanowire pores yield larger peak power factors. We note that such large confinement may be produced by a thin layer of high-potential barrier material such as an oxide layer.³¹ In addition, we show that larger cross-sectional ratios, d/δ , can produce significantly larger peak power factors. However, we note that samples with large d/δ and with d in the region of peak P_{ncm} are more difficult to fabricate because they require very small δ . Furthermore, in real systems large cross-sectional ratio can be achieved only if the nanowire pores are themselves large. This would mean that in the full nanowire-composite structure the power factor of the nanowire material filling the pores would not benefit from any confinement-induced enhancement. This suggests that an optimum cross-sectional ratio must be found to maximize power factor enhancement in both the nanowires and in the surrounding matrix region.

¹L. D. Hicks and M. S. Dresselhaus, Phys. Rev. B **47**, 12727 (1993).

²L. D. Hicks and M. S. Dresselhaus, Phys. Rev. B **47**, 16631 (1993).

³R. Venkatasubramanian, E. Siivola, T. Colpitts, and B. O'Quinn, Nature (London) **413**, 597 (2001).

⁴T. C. Harman, P. J. Taylor, M. P. Walsh, and B. E. LaForge, Science **297**, 2229 (2002).

⁵T. E. Humphrey and H. Linke, Phys. Rev. Lett. **94**, 096601 (2005).

⁶A. R. Abramson, W. C. Kim, S. T. Huxtable, H. Yan, Y. Wu, A. Majumdar, C.-L. Tien, and P. Yang, J. Microelectromech. Syst. **13**, 505 (2004).

⁷J. R. Lim, J. F. Whitacre, J.-P. Fleurial, C.-K. Huang, M. A. Ryan, and N. V. Myung, Adv. Mater. (Weinheim, Ger.) **17**, 1488 (2005).

⁸Yu-Ming Lin and M. S. Dresselhaus, Phys. Rev. B **68**, 075304 (2003).

⁹K. F. Hsu, S. Loo, F. Guo, W. Chen, J. S. Dyck, C. Uher, T. Hogan, E. K. Polychroniadis, and M. G. Kanatzidis, Science **303**, 818 (2004).

¹⁰J. O. Sofo and G. D. Mahan, Appl. Phys. Lett. **65**, 2690 (1994).

¹¹D. A. Broido and T. L. Reinecke, Phys. Rev. B **51**, 13797 (1995).

¹²D. A. Broido and T. L. Reinecke, Appl. Phys. Lett. **70**, 2834 (1997).

¹³L. D. Hicks, T. C. Harman, X. Sun, and M. S. Dresselhaus, Phys. Rev. B **53**, R10493 (1996).

¹⁴T. Koga, T. C. Harman, S. B. Cronin, and M. S. Dresselhaus, Phys. Rev. B **60**, 14286 (1999).

¹⁵D. A. Broido and T. L. Reinecke, Appl. Phys. Lett. **77**, 705 (2000).

¹⁶D. A. Broido and T. L. Reinecke, Phys. Rev. B **64**, 045324 (2001).

¹⁷N. Mingo, Appl. Phys. Lett. **84**, 2652 (2004).

¹⁸N. Mingo and D. A. Broido, J. Appl. Phys. (to be published).

- ¹⁹We ignore the band bending produced by the carriers and by electrostatic potential from the ionized impurities that provides them.
- ²⁰See, for example, B. R. Nag, *Electron Transport in Compound Semiconductors* (Springer-Verlag, Berlin, 1980).
- ²¹C. Kittel, *Introduction to Solid State Physics*, 8th ed. (Wiley, 2005), Chap. 7.
- ²²H. Rucker, E. Molinari, and P. Lugli, Phys. Rev. B **45**, 6747 (1992).
- ²³P. A. Knipp and T. L. Reinecke, Phys. Rev. B **48**, 18037 (1993).
- ²⁴We note that these expressions are identical to those derived previously for quantum wire superlattices in Ref. 16. We include them here for completeness.
- ²⁵While the narrow energy gap in InSb causes its conduction band to be strongly non-parabolic, previous calculations by us (Ref. 18) including this non-parabolicity did not show dramatic differences from those obtained in the parabolic approximation.
- ²⁶D. L. Rode, Phys. Rev. B **3**, 3287 (1971).
- ²⁷Landolt Börnstein, *Numerical Data and Functional Relationships in Science and Technology, New Series*, Vol. 17e (Springer-Verlag, Berlin, 1982), pp. 218–258.
- ²⁸G. Nimtz and B. Schlicht, *Narrow-Gap Semiconductors* (Springer-Verlag, Berlin, 1982), pp. 1–106.
- ²⁹H. Yokoi, S. Takeyama, N. Miura, and G. Bauer, Phys. Rev. B **44**, 6519 (1991).
- ³⁰For the large d limit, several hundred subbands are involved, and the inelastic pop intersubband scattering becomes prohibitively difficult to treat.
- ³¹S. B. Cronin, Y.-M. Lin, O. Rabin, M. R. Black, and M. S. Dresselhaus, in *The 21st International Conference on Thermoelectrics: ICT Symposium Proceedings, Long Beach, CA*, edited by T. Caillat and J. Snyder (Institute of Electrical and Electronics Engineers, Piscataway, NJ, 2002), pp. 243–248.